

On the age vs depth and optical clarity of deep ice at South Pole

The AMANDA collaboration*

Abstract

The first four strings of phototubes for the AMANDA high-energy neutrino observatory are now frozen in place at a depth of 800 to 1000 m in ice at the South Pole. During the 1995-96 season an additional six strings will be deployed at greater depths. Provided absorption, scattering, and refraction of visible light are sufficiently small, the trajectory of a muon into which a neutrino converts can be determined by using the array of phototubes to measure the arrival times of Čerenkov light emitted by the muon. To help in deciding on the depth for implantation of the six new strings, we discuss models of age vs depth for South Pole ice, we estimate mean free paths for scattering from bubbles and dust as a function of depth, and we assess distortion of light paths due to refraction at crystal boundaries and interfaces between air-hydrate inclusions and normal ice. We conclude that the depth interval 1600 to 1800 m will be suitably transparent for the next six AMANDA strings and, moreover, that the interval 1600 to 2100 m will be suitably transparent for a future 1-km³ observatory except possibly in a region a few tens of meters thick at a depth corresponding to a peak in the dust concentration at 60 kyr BP.

INTRODUCTION

With the creation of AMANDA (the Antarctic Muon and Neutrino Detector Array), we hope to open a new astronomical window, using neutrinos instead of light (Lowder and others, 1991; Barwick and others, 1992). The goal is to image the trajectories of ultrahigh-energy neutrinos created throughout the universe in very energetic processes such as take place in quasars and other Active Galactic Nuclei. Because the conversion of neutrinos into detectable particles is extremely small, the observatory must be huge, eventually of order 1 km^3 in volume. All designs share the same idea: a three-dimensional array of large phototubes embedded in a transparent medium will look down at the cone of Čerenkov light emitted by an upward-moving muon into which a high-energy neutrino is transformed in passing upward through the Earth. Measurement of arrival times of Čerenkov photons at various phototubes enables the direction of the neutrino to be reconstructed. In contrast to other techniques, which propose to build an observatory in a deep lake or the deep ocean, all of the electronics in the present version of AMANDA sit on the surface of South Pole ice above cables that simply carry signals up from the phototubes, and the imaging medium is essentially free of background light such as that due to radioactivity or bioluminescence.

To minimize cost, the strings of phototubes should be far apart and the spacing of phototubes on each string should be large. To reduce background due to downward- directed muons created in the Earth's atmosphere, the array should be buried deeply and the phototube spacing should be large in order to give a long enough lever arm to determine trajectories very accurately. Our results from the first four strings, which were deployed during the 1993-94 drilling season, showed that Čerenkov light from downward muons propagated diffusively due to scattering from residual air bubbles at the depth interval 800 to 1000 m where the phototubes were located (Askebjerg and others, 1994). Using a laser to send pulses of light (500 nm) down optical fibers to various depths, we measured the distribution of arrival times at phototubes at various distances from the emitter. From the excellent fits to a model of random walk with absorption, we were able to determine separately the absorption length (the e-folding distance for loss of photons at a particular wavelength) and the scattering length (the mean free path between scatterers). The result for the absorption length at 500 nm, $\lambda_{abs} = 59 \pm 3 \text{ m}$, is larger than that of the clearest ocean water and far larger than the values estimated for laboratory ice and for Lake Baikal. This large value of λ_{abs} will permit us ultimately to construct a neutrino observatory at lower cost than we originally expected. The geometrical scattering length on bubbles, λ_{bub} , was found to be 11 cm at 800 m and to increase to 26 cm at 1000 m. In order to take maximum advantage of the information from Čerenkov wavefront arrival times, we plan to implant all future strings of AMANDA phototubes at depths sufficiently great that λ_{bub} is greater than about 20 m.

Figure 1 is a sketch showing the location of the first four AMANDA strings and the proposed location of the remaining six strings. In this paper we discuss the factors that must be considered in deciding how deep to implant the remaining six strings. Future plans to proceed to construction of a 1 km^3 -size neutrino observatory will depend on success in deploying these six strings and on results of measurements with them.

TIME-SCALE MODEL (AGE VS. DEPTH)

To estimate the dust concentration as a function of depth, we require a model of age as a function of depth for South Pole ice. The most important ingredient of such a model is the accumulation rate as a function of time and distance upstream from the site. Since very little information on accumulation rate upstream from the South Pole has been published, there is little point in developing a sophisticated flowline model. We start with the information in Table 1 on deep cores in ice and on drilling sites. The first four rows are for Greenland sites and the last four are for Antarctic sites. The last row includes information about the South Pole site. No core deeper than 349 m has been obtained at this site.

Figure 2 displays age vs depth obtained from references at the bottom of Table 1. Wherever possible, we

selected data based on absolute determination of age using stratigraphy (annual layers of high and low $\delta^{18}\text{O}$ values, of electrical conductivity, of dust, or of dissolved impurities due, for example, to identifiable volcanic eruptions). In other cases we followed the authors in associating patterns of $\delta^{18}\text{O}$, ^{10}Be , and dust concentrations from core to core with dated events such as the Last Glacial Maximum. To complete the picture, we selectively used ages based on ice-flow models reported by the various authors. In case of any discrepancies from one author to another, we used the most recent work or the one least dependent on flow models. For the Camp Century core, ages estimated from Fourier spectral analyses of $\delta^{18}\text{O}$ profiles and comparisons with features in the deep sea record differ by a factor ~ 2 for times greater than ~ 10 kyr. Various reasons have been given for the irregularities in the Camp Century time-scale near the bottom of the core (Dansgaard and others, 1982). We decided to include only the data for depths more than 280 m above bedrock, for which stratigraphy is said to be accurate to $\pm 3\%$ (Hammer and others, 1978).

Figure 3 casts the data in Fig. 2 as a universal function in which depth as a function of age is shown in dimensionless coordinates. The dimensionless time is defined as $t^* \equiv t a(t)/H$, where t is the time in years, a is the accumulation rate in meters of ice (at density 0.92 g cm^{-3}) per yr, and H is the ice thickness (m) to bedrock. The dimensionless depth is defined as $d^* \equiv d/H$. Following the practice of most authors, for times $t < 15$ kyr BP we took $a(t)$ to be its average value during the Holocene, and for $15 \leq t \leq 110$ kyr BP we took $a(t)$ to be a constant fraction of its Holocene value. For Antarctic sites, the fraction is taken to be 0.75; for Greenland sites the fraction is taken to be 0.5. Our adopted values of $a(t)$ are given in columns 7 and 8 of Table 1. The rationale for assigning a smaller value to $a(t)$ during the period 15 to 110 kyr BP is that large portions of the time-scales given in the references are based on ice-flow models for which the authors (with justification) assumed a smaller value of $a(t)$ during that period. This approach should be most successful for sites near ice divides, for which the horizontal flowrate is small. Recently more sophisticated models have been used, in which the accumulation rate has been taken as continuously varying in a way that can be inferred from the ^{18}O record or the ^{10}Be record less the spikes. Since such data are not available for South Pole ice, we have contented ourselves with the simpler approach using step-function values as described above. For the South Pole site, with its large horizontal flowrate, the accumulation rate far upstream, from which the deep ice originated, is somewhat smaller than assumed in our simple model (Mosley-Thompson, 1994). To convey an idea of the uncertainty, we will present two age vs depth curves for the South Pole, one of which (McInnes and Radok, 1984) is based on very low upstream accumulation rates.

Analytical ice flow models of age vs depth have evolved from work by Nye (1963), Weertman (1968), and Dansgaard and Johnsen (1969). On the assumption of a constant vertical strain-rate with depth, Nye (1963) found the simple dependence of depth on age:

$$d = H(1 - \exp(-at/H)) \quad (1)$$

where $a = \text{constant}$. In the dimensionless version,

$$d^* = 1 - \exp(-t^*). \quad (2)$$

More refined models take into account the variation of horizontal flowrate, vertical strain-rate, and temperature with depth; the dependence of ice plasticity on temperature and crystal texture; the temperature at the ice-bedrock interface; the flow paths of ice from the surface at various times in the past to its present depth, which depends on factors such as the distance of the core from an ice divide; the variation of accumulation rate upstream as a function of time and of the position from which the ice originated; the slope of the bedrock; and the slope at the surface. Little of this information is available for the South Pole site.

The universal curve in Fig. 3 is for eq. 2. One sees that for values of reduced depth d^* greater than about 0.5 the scatter becomes large. With the universal curve as input, the solid curve in Fig. 4 shows our

prediction of the age vs depth for the South Pole. The best direct measurements give quite consistent values of accumulation rate for recent times: $a = 0.074$ m/yr from annual dust layers extending back to 1590 A.D. (Mosley-Thompson, 1994), $a = 0.072$ m/yr based on visible stratigraphy in an inclined snow mine for the period 1950 to 1770 A.D. (Giovinetto, 1964), and 0.073 m/yr based on a stake network and beta-activity measurements over much of Antarctica (Young and others, 1982). The solid curve in Fig. 4 is for $a(t) = 0.073$ m/yr back to 15 kyr BP and 0.055 m/yr before 15 kyr BP.

One attempt to predict age vs depth for ice at the South Pole has been published (McInnes and Radok, 1984). The dashed curve in Fig. 4 shows their model, which agrees with ours at depths down to ~ 1300 m, corresponding to an age of ~ 33 kyr BP. For greater depths they inferred a much more rapid increase in age with depth than we do, because they assumed an abrupt decrease in accumulation rate from ~ 0.088 m/yr at the Pole to a constant value of ~ 0.02 m/yr for ice more than ~ 100 km upstream, which reaches the Pole at times greater than ~ 30 kyr BP. Mosley-Thompson's recent measurements of accumulation rate at Plateau Remote, near the Pole of Relative Inaccessibility, gave values about twice as large as assumed by McInnes and Radok. The two curves in Fig. 4 give, with high probability, upper and lower limits on the true values.

The irregular curve along the abscissa gives the dust flux at South Pole in arbitrary units as a function of time, inferred from measurements made on an ice core at Vostok (See later section for discussion).

DEPTH DEPENDENCE OF SCATTERING FROM BUBBLES

A quantity of great relevance to the AMANDA project is the depth-dependence of λ_{bub} , the mean free path for scattering of the visible component of Čerenkov radiation off of air bubbles. For smooth spherical bubbles of rms radius r and number concentration n , $\lambda_{bub} = (n\pi r^2)^{-1}$. For purposes of discussion, the polar ice can be divided into three depth regimes: At depths shallower than the closeoff depth (typically ~ 60 m), the firn is porous to air. At intermediate depths, bubbles exist at an approximately constant number concentration and with mean bubble volume that decreases as hydrostatic pressure increases. At great depths, bubbles transform into a more stable phase consisting of air hydrate crystals.

Bubbles are formed at the "closeoff" depth at which the firn changes into ice. The volume fraction of air trapped in the ice at pore closeoff, V_c , is given experimentally (Raynaud and Lebel, 1979) by

$$V_c(\text{cm}^3/\text{g of ice}) = (2 \times 10^{-4} - 0.015/T(K))P(\text{mbar}) \quad (3)$$

V_c depends on atmospheric pressure and thus on altitude at the time of closeoff, and depends weakly on temperature. For Vostok, $V_c = 0.084$ cm³/g, whereas for Byrd, at an altitude nearly 2000 m lower than Vostok, $V_c = 0.114$ cm³/g. The South Pole, with altitude intermediate between Vostok and Byrd, should have an intermediate value of V_c .

At z_c , the ice-equivalent depth for pore closeoff, $\rho V_c/n = 4\pi r^3/3$ if all the gas is in bubbles (where ρ = mass density). The number concentration at pore closeoff depends on temperature, dust concentration, and other climatic factors, but is roughly similar for Vostok and Byrd, the two cores in which detailed studies have been made of bubbles. Since the ice density is roughly constant below the firn layer and the ice temperature does not change much in the first 1000 m, the perfect gas law leads to expressions for the depth dependence of the rms bubble radius

$$r = \left(\frac{3\rho V_c z_c}{4\pi n z}\right)^{1/3} \quad (4)$$

and of $1/\lambda_{bub}$:

$$1/\lambda_{bub} = \left(\frac{3\rho V_c z_c n^{1/2} \pi^{1/2}}{4z} \right)^{2/3} \quad (5)$$

The latter is shown by the solid curve in Fig. 5. The figure also shows data for $1/\lambda_{bub}$ at Byrd, Vostok, and the South Pole, derived from measurements by Gow and Williamson (1975) on a Byrd core, by Barkov and Lipenkov (1984) on a Vostok core, and on laser calibration data in situ by the AMANDA collaboration (Askebjør and others, 1994). The vertical dashed lines for the in situ measurements are put in to remind the reader that the scattering length inferred from the data depends on the angular distribution of scattered light: the lower triangles correspond to the assumption of isotropic scattering from bubbles with rough surfaces, which might come about, for example, if air hydrate crystals were nucleating at various points on the surfaces) and the upper triangles correspond to the assumption of forward-peaked scattering from smooth, spherical bubbles. (The true values should lie somewhere in between.) The curve in Fig. 5 is normalized to the data at depths less than 700 m by choosing $z_c = 15$ m.

At depths from 100 to nearly 700 m the data for Byrd and Vostok follow the hydrostatic pressure curve rather well. At greater depths the inverse scattering length decreases rapidly with depth, due to a decrease in n brought about by a phase transition. A quantitative diffusion-growth model for the conversion of bubbles into air hydrate crystals (Price, 1994) both fits the data for $1/\lambda_{bub}$ as a function of depth at Vostok and Byrd and predicts the effective disappearance of bubbles at a depth of ~ 1450 m in South Pole ice. The dotted curves in Fig. 5 show the results of that calculation for Vostok and Byrd and the dashed curve shows the prediction for the South Pole. In the next section we discuss further the phase transition from the two-phase system (ice + bubbles) into the two-phase system (ice + air hydrate).

CONVERSION OF BUBBLES TO AIR HYDRATE CRYSTALS

Miller (1969) first showed that, at sufficiently high pressure, the system (air bubbles + ice) become unstable against the transformation into a two-phase system consisting of normal ice + crystals of the cubic clathrate ice structure in which O_2 and N_2 molecules occupy a fraction of the clathrate cages (experimentally, about 80%). In Fig. 6 the dashed curves (Miller, 1969) give the dissociation pressures as a function of ice temperature for nitrogen hydrate and "air hydrate". Within the hatched region between the two curves both bubbles and hydrate crystals should co-exist. On the same graph we show the temperature as a function of depth for some cores for which either measurements or calculations exist. The profile at South Pole is based on a model with T fixed at -50° C at the surface and at the pressure-melting temperature at bedrock. Seven months after completion of hot-water drilling, temperatures measured at 800 to 1000 m with thermistors imbedded during the AMANDA operation had dropped to within $\sim 0.3^\circ$ C of the model temperatures.

With polarized light, air hydrate crystals have been observed in a number of core sections. Shoji and Langway (1982; 1987) studied air hydrate crystals in cores from Dye 3, Camp Century, and Byrd Station. Uchida and others (1994) recently made quantitative measurements of size, shape, and concentration of such crystals as a function of depth in Vostok cores. In Fig. 6 we have indicated on the depth vs temperature curves the depths at which air hydrate crystals first appear, as well as the depths at which air bubbles are no longer present. Shoji and Langway (1987) pointed out that the depth at which air hydrate crystals first appear agrees reasonably well with the depths corresponding to the dissociation pressures calculated for air hydrate by Miller (1969). To explain why air hydrate crystals are found at depths about 100 m above the depth corresponding to the equilibrium phase boundary at Byrd (see our Fig. 6), Craig and others (1993) pointed out that the hydrate crystals had probably formed at a greater depth just upstream of Byrd and had remained metastable following vertical advection of ice through the local phase- boundary depth on the way to their present location at Byrd. The advection is attributed to large-scale irregularities in the topography

of the bedrock. Since the bedrock topography upstream of South Pole would not give rise to such upwelling, we predict that air hydrates will appear in increasing concentration at depths exceeding ~ 500 m at the South Pole.

Price (1994) showed that the broad transition zone in depth for coexistence of both bubbles and air hydrate crystals in ice cores was due not to a nucleation barrier but rather to the slowness of diffusion of water molecules through a spherical shell of air hydrate crystal forming on bubble walls. His model exploited the fact that, whereas the activation energy for diffusion through normal ice is only 0.57 eV, the activation energy for diffusion through air hydrate is much higher, 0.9 eV (Uchida and others, 1992), which is able to account for the very slow growth rate of air hydrate crystals.

In Table 1, column 9 gives the depths at which air bubbles in various cores are no longer seen. The same data are displayed in Fig. 6. For the South Pole site, we adopt the diffusion model that predicts essentially complete conversion of bubbles into air hydrate crystals at depths greater than 1450 m.

DUST VS DEPTH

In the absence of bubbles, insoluble dust particles with diameters ~ 0.1 to ~ 10 μm make the most important contribution to scattering of visible light in the ice. The concentration of dust and soluble impurities in the ice has been shown to be directly related to the concentration of atmospheric aerosols. The size distribution is log normal, with typical modal diameter ranging from 0.5 μm (in Dome C: Royer and others, 1983) to 0.6 μm (in Vostok: De Angelis and others, 1984). The dust concentration in ice cores shows both an annual variation and a long-term anticorrelation with the temperature inferred from $\delta^{18}\text{O}$ measurements. For example, as seen in Table 2, all deep cores show an increase in dust concentration at depths corresponding to the Last Glacial Maximum – by one order of magnitude for Antarctica and by two orders of magnitude for Greenland. The vertical dust flux increases as global temperature decreases, both because of increased continental aridity and because of higher wind velocity. (The flux is roughly proportional to the desert area of nearby continents and to the cube of wind velocity.) For a given annual dust flux the concentration deposited in ice is inversely proportional to snow accumulation rate and is roughly constant for the entire Antarctic continent (Petit and others, 1990).

In Fig. 4, the irregular curve shows the dust flux as a function of time at Vostok inferred from measurements on an ice core (Petit and others, 1990). By comparing this curve with the two models of age vs depth on the same graph, we obtain estimates of the depths at the South Pole at which maxima and minima in the dust concentration occur. For example, both of the two models predict that the largest peak, corresponding to the Last Glacial Maximum, will be found at a depth of ~ 1000 m. The next maximum, at ~ 60 kyr BP, is predicted to occur at ~ 1950 m with the AMANDA model shown by the solid curve and at ~ 1500 m with the McInnes-Radok model (dashed curve).

Taking together the requirements that all bubbles must have converted into air hydrate crystals (which dictates that the detectors be deeper than 1450 m), that depths with high dust concentration be avoided, and that depths of large horizontal shear (> 2100 m) be avoided, the two models lead to the following constraints:

- With the "AMANDA" model given by the solid curve, the longest scattering lengths are to be found at 1450 m to 1850 m.
- With the McInnes-Radok model given by the dashed curve, the longest scattering lengths are to be found at 1600 to 2100 m.

Thus, with either model a ~ 250 -m-long vertical string of detectors would encounter a low dust concentration

at 1600 to 1850 m. In planning for an eventual 1-km³ array it would be useful to use the pulsed laser technique to measure λ_{scat} as a function of depth throughout the region of possible interest from 1450 to 2100 m. As the AMANDA observatory expands beyond the set of ten strings envisaged in Fig. 1, additional strings can be implanted so as to avoid the dust peak at 60 kyr BP.

We next estimate the mean free path for light scattering from dust at the South Pole for the maximum and minimum values of the dust concentration. We use data collected in Table 2, which gives our estimates of the dust concentrations in various cores at depths corresponding to three times: the Holocene (from the present back to ~ 13 kyr BP), for which the dust concentration has been roughly constant and quite low; the Last Glacial Maximum, at ~ 18 kyr BP; and a time ~ 40 kyr BP, typical of the region of minimal dust concentration. Data at the South Pole exist only for a depth of 100 to 349 m (Mosley-Thompson, 1994). To predict the concentration at 40 kyr BP at South Pole, we note that the ratio of the concentration at 40 kyr BP and during the Holocene is ~ 1.5 for Byrd, 2.6 for Dome C, and 2.9 for Vostok. We assume that the average of these three values, a factor 2.3, holds at South Pole. Noting that the ratio of concentrations at LGM and during the Holocene is 10, 17, and 12 for Byrd, Dome C, and Vostok respectively, we adopt a factor ~ 13 for the South Pole. Our predictions appear in row 6 of Table 2.

We estimate the mean free path for light scattering from dust in two ways. The more direct approach uses the data in Table 3 on the diameter distribution of dust measured in an ice core in the depth interval 100 to 349 m at South Pole. (No deeper core has yet been obtained.) Column 2 gives the numbers of particles per ml and column 3 gives the total cross-sectional area per ml assuming πr^2 per particle. Summing the entries gives 7×10^4 particles with diameter $> 0.1 \mu\text{m}$ and total cross-sectional area per ml of $7 \times 10^{-5} \text{ cm}^{-1}$. (For a log-normal size distribution peaked at $0.5 \mu\text{m}$, the area/ml below $0.1 \mu\text{m}$ (Gayley and Ram (1985) is negligible and the area/ml above $2 \mu\text{m}$ (Mosley-Thompson, 1994) is as given in Table 3.) The reciprocal of the latter quantity is the mean free path, λ_{scat} , which is seen to be ~ 140 m. Assuming that the relative concentrations in the different diameter intervals do not change with depth, we can scale the mean free path to different times, leading to the prediction that $\lambda_{scat} \sim 11$ m at the Last Glacial Maximum and $\lambda_{scat} \sim 60$ m at a depth corresponding to 40 kyr BP.

The second approach is based on the study of light scattering and absorption by dust suspended in a Dome C core. Royer et al. (1983) used a gonionephelometer to measure the intensity of light at 546 nm scattered at angles from 15° to 150° in freshly melted ice. Using Mie theory to fit the angular distribution of scattered light, they derived average values of the scattering coefficient $b = 3.46 \pm 0.2 \times 10^{-2} \text{ m}^{-1}$ for Holocene samples, $b = 10 \pm 2.5 \times 10^{-2} \text{ m}^{-1}$ for LGM samples, and $\sim 5 \times 10^{-2} \text{ m}^{-1}$ for samples near the bottom of the core (corresponding to ~ 30 kyr BP). From these results we infer a mean free path $\lambda_{scat} = 20$ m for dust near the bottom of the core at Dome C. Scaling with accumulation rate, we infer $\lambda_{scat} = 40$ m for dust at 1500 m at South Pole. Comparison of this result with that obtained by the first approach provides an indication of the uncertainty in the value of λ_{scat} .

REFRACTION BY AIR HYDRATE CRYSTALS

In the last section we concluded that in the depth interval 1600 to 1850 m at the South Pole all bubbles will have transformed into air hydrate crystals and λ_{scat} will be of order 40 to 60 m, independent of the age vs depth model. Because the air hydrate crystals have dimensions very large relative to the wavelength of light, Čerenkov light will undergo refraction rather than scattering at interfaces between air hydrate and hexagonal ice crystals. The quantitative effect of the hydrate crystals on light transmission will depend on their size, shape, concentration, and refractive index relative to that of the normal ice in which they are imbedded. Using X-ray diffraction, Hondoh and others (1990) verified the cubic clathrate nature of natural air hydrate crystals in a Dye 3 deep core. From the Raman intensities of the stretching modes of N₂ and O₂, Nakahara and others (1988) inferred a composition ratio of N₂ to O₂ to be 1.6 - 1.9 in the clathrate

structure of these same hydrate crystals. Shoji and Langway (1982; 1987) made optical studies and did laboratory experiments on air hydrate crystals in ice cores from Dye 3, Camp Century, and Byrd. Uchida (1994) determined that the ratio of the refractive index of natural air hydrate in ice core samples relative to the refractive index of hexagonal ice is 1.004. Uchida and others (1994) recently made an extensive study of the depth profiles of the shape, volume concentration, number concentration, and mean volume per crystal of air hydrate crystals in Vostok ice-core samples. They found a typical concentration of air hydrate crystals of $\sim 500 \text{ cm}^{-3}$, a typical diameter of $\sim 100 \mu\text{m}$, and a predominance of spherical shapes, from which we infer a typical mean path of $\sim 25 \text{ cm}$ for encounter of a light ray with such crystals. To reach a phototube at a distance of, say, 25 m requires $\sim 10^2$ traversals of such crystals. For a typical angle of incidence of 45° and 10^2 encounters, and taking into account refraction at both entrance and exit with $n = 1.004$, the net lateral deflection due to a random walk about the initial direction would be only $\sim 5 \text{ cm}$ over the 25 m pathlength. Thus, because of the nearly perfect match of refractive index to that of hexagonal ice, air hydrate crystals have virtually no effect on the imaging of muon trajectories.

REFRACTION AT ICE CRYSTAL BOUNDARIES

With its hexagonal crystal structure, ice has a refractive index along the c-axis that is larger than that in the basal plane by a factor of 1.001. Assuming a mean crystal size of 4 mm, the same as measured in the Vostok core at a depth of 1500 m (Lipenkov and others, 1989), a light ray in South Pole ice would refract ~ 6000 times in traversing a distance of 25 m. To make the most conservative estimate, we assume a random distribution of c-axes with a typical angle of 45° between c-axes in adjacent crystals. Then the net deflection due to a random walk of 6000 steps would be only $\sim 0.2 \text{ cm}$ over the 25 m pathlength. Again, we are helped by the very small ratio of refractive indices across a crystal boundary.

CONCLUSIONS

1. Almost certainly the true age vs depth relationship lies between the two curves in Fig. 4. The AMANDA model (solid curve) probably underestimates ages at great depths because the choice of $a(t) = 0.055 \text{ m/yr}$ during the interval 15 to 110 kyr BP is higher than recent values estimated by Mosley-Thompson (1994). The flowline model of McInnes- Radok (dashed curve) overestimates the ages at depths greater than $\sim 1300 \text{ m}$ because of the very small assumed value $a(t) = 0.02 \text{ m/yr}$ at distances more than $\sim 180 \text{ km}$ upstream.
2. A diffusion-growth model that fits Vostok and Byrd core data predicts that the transformation of bubbles into air hydrate crystals at the South Pole will be complete at depths below $\sim 1450 \text{ m}$.
3. Using data on the size distribution of dust in a shallow South Pole core (100 to 349 m) together with systematics of depth profiles of dust concentrations at other sites, we estimate a mean free path of ~ 40 to $\sim 60 \text{ m}$ for scattering of light from dust in the depth interval 1600 to 1850 m at South Pole. In this depth interval both age models give the same result. At the depth corresponding to the peak in the dust concentration at $\sim 60 \text{ kyr BP}$, the scattering mean free path is estimated to drop to ~ 13 to 20 m . Such short mean free paths are confined to a vertical layer a few tens of meters thick located somewhere between 1500 and 2000 m depending on the age vs depth model.
4. Taking into account the age vs depth relationship, the depth profile of the dust concentration for the deep Vostok core, the expected depth for bubble disappearance (1450 m), and the depth ($\sim 2500 \text{ m}$) at which the horizontal ice flow rate is thought to change rapidly with depth (Koci, 1994), we conclude that
 - the next six AMANDA strings should be implanted at a depth of 1600 to 1850 m;

- the future 1-km³ observatory could extend vertically from 1600 to 2100 m, with a horizontal area of ~ 2 km². Once the layer of high dust concentration has been located with the pulsed laser technique, one could simply exclude data recorded in phototubes in this layer a few tens of meters thick.
5. Due to the small difference in refractive index between air hydrate and normal hexagonal ice crystals, refraction at the interfaces between the two types of crystals will have a negligible effect on the trajectories of Čerenkov light rays emitted by muons in the ice.
 6. Similar reasoning leads to the conclusion that, due to the small difference in refractive index parallel to and perpendicular to the c-axis in normal hexagonal ice, refraction at the interfaces between randomly distributed ice crystals will have a negligible effect on the trajectories of Čerenkov light rays emitted by muons.

ACKNOWLEDGMENTS

We are indebted to Bruce Koci and the entire PICO organization for their excellent support with the ice drilling. This work was supported in part by the National Science Foundation, the K. A. Wallenberg Foundation, the Swedish Natural Science Research Council, the G. Gustafsson Foundation, Swedish Polar Research, and the Graduate School of the University of Wisconsin, Madison. We thank R. B. Alley, S. P. Davis, P. Duval, J. Fitzpatrick, A. J. Gow, T. Hondoh, B. Koci, V. Ya. Lipenkov, S. L. Miller, E. Mosley-Thompson, R. G. Pain, J. M. Palais, J. R. Petit, M. Ram, C. F. Raymond, and T. Uchida for helpful discussions.

★ Members of the AMANDA Collaboration are P. Askebjerg*, S. Barwick†, L. Bergström, A. Bouchta*, S. Carius‡, A. Coulthard§, K. Engel§, B. Erlandsson*, A. Goobar*, L. Gray§, A. Hallgren‡, F. Halzen§, P. O. Hulth*, J. Jacobsen§, S. Johansson*¶, V. Kandhadai§, I. Liubarsky§, D. Lowder&, T. Miller&**, P. Mock†, R. Morse§, R. Porrata†, P. B. Price&, A. Richards&, H. Rubinstein‡, J. C. Spang§, Q. Sun*, S. Tilav§, C. Walck*, and G. Yodh†. For communication regarding this manuscript, correspond with P. B. Price (e-mail address price@lbl.gov).

*Stockholm University, Sweden

†University of California, Irvine, CA

‡Uppsala University, Sweden

§University of Wisconsin, Madison, Wisconsin

&University of California, Berkeley, CA

¶Currently at Jönköping University, Sweden

**Currently at Bartol Research Institute, Delaware

REFERENCES

- Askebjerg, P., and others. 1994. *Science*, in press.
- Barkov, N. I., and V. Ya. Lipenkov. 1984. *Mat. Glyatsiol. Issled.* **51**, 178-186.
- Barwick, S., F. Halzen, D. Lowder, T. Miller, R. Morse, P. B. Price, and A. Westphal. 1992. *J. Phys. G: Nucl. Part. Phys.* **18**, 225-247.
- Craig, H., H. Shoji, and C. C. Langway, Jr. 1993. *Proc. Natl. Acad. Sci.* **90**, 11416.
- Dahl-Jensen, D. 1989. *Ann. Glaciology* **12**, 31-36.
- Dahl-Jensen, D., and S. J. Johnsen. 1986. *Nature* **320**, 250-252.
- Dansgaard, W., and S. J. Johnsen. 1969. *Journal of Glaciology* **8** (53), 215-223.
- Dansgaard, W., H. B. Clausen, N. Gundestrup, C. U. Hammer, S. F. Johnsen, P. M. Kristinsdottir, and N. Reeh. 1982. *Science* **218**, 1273-1277.
- Dansgaard, W., S. J. Johnsen, H. B. Clausen, D. Dahl-Jensen, N. Gundestrup, C. U. Hammer, C. S. Hvidberg, J. P. Steffensen, A. E. Sveinbjörnsdottir, J. Jouzel, and G. Bond. 1993. *Nature* **364**, 218-220.
- De Angelis, M., M. Legrand, J. R. Petit, N. I. Barkov, Ye. S. Korotkevich, and V. M. Kotlyakov. 1984. *Journal of Atmospheric Chemistry* **1**, 215-239.
- Gayley, R. I., and M. Ram. 1985. *Journal of Geophysical Research* **90**, 12921-12925.
- Giovinetto, M. B. 1964. *Antarctic Research Series (American Geophysical Union)*, **2**, 127-155.
- Gow, A. J., and T. Williamson. 1975. *Journal of Geophysical Research* **80**, 5101-5108.
- Hammer, C. U., H. B. Clausen, W. Dansgaard, N. Gundestrup, S. J. Johnsen, and N. Reeh. 1978. *Journal of Glaciology* **20**, 3-26.
- Hondoh, T., H. Anzai, A. Goto, S. Mae, A. Higashi, and C. C. Langway, Jr. 1990. *Journal of Inclusion Phenomena and Molecular Recognition in Chemistry* **8**, 17-24.
- Ikeda, T., T. Uchida, and S. Mae. 1993. *Proc. NIPR Symp. Polar Meteorol. Glaciol.* **7**, 14-23.
- J. Jouzel et al. 1993. *Nature* **364**, 407-412.
- Kittel, C. and H. Kroemer. 1980. Thermal Physics, second edition (W. H. Freeman, San Francisco).
- Koci, B. 1994. Private communication.
- Lipenkov, V. Ya., N. I. Barkov, P. Duval, and P. Pimienta. 1989. *Journal of Glaciology* **35**, 392-398.
- Lorius, C., L. Merlivat, J. Jouzel, and M. Pourchet. 1979. *Nature* **280**, 644-648.
- Lorius, C., D. Raymond, J. R. Petit, J. Jouzel, and L. Merlivat. 1984. *Ann. Glaciology* **5**, 88-94.
- Lorius, C., J. Jouzel, C. Ritz, L. Merlivat, N. I. Barkov, Y. S. Korotkevich, and V. M. Kotlyakov. 1985. *Nature* **316**, 591-596.
- Lowder, D., T. Miller, P. B. Price, A. Westphal, S. W. Barwick, F. Halzen, and R. Morse. 1991. *Nature* **353**, 331-333.

- McInnes, B. and U. Radok. 1984. *Antarctic Journal of the U. S.* **19** (1), 10-12.
- Miller, S. L. 1969. *Science* **165**, 489-490.
- Mosley-Thompson, E. 1994. Private communication.
- Mosley-Thompson, E., and L. G. Thompson. 1982. *Quaternary Research* **17**, 1-13.
- Nye, J. F. 1963. *Journal of Glaciology* **4** (36), 785-788.
- Nakahara, J., Y. Shigesato, A. Higashi, T. Hondoh, and C. C. Langway, Jr. 1988. *Philosophical Magazine* **57**, 421-430.
- Palais, J. M., M. S. Germani, and G. A. Zielinski. 1992. *Geophysical Research Letters* **19** (8), 801-804.
- Petit, J. R., M. Briat, and A. Royer. 1981. *Nature* **293**, 391-394.
- Petit, J. R., L. Mounier, J. Jouzel, Y. S. Korotkevich, V. I. Kotlyakov, and C. Lorius. 1990. *Nature* **343**, 56-58.
- Price, P.B. 1994. *Science*, in press.
- Raynaud, D., and B. Lebel. 1979. *Nature* **281** (5729), 289-291.
- Ritz, C. 1989. *Ann. Glaciology* **12**, 138-144.
- Robin, G. deQ. 1983. In Climate Record in Polar Ice Sheets (Cambridge University Press, New York), Chap. 4.
- Royer, A., M. De Angelis, and J. R. Petit. 1983. *Climatic Change* **5**, 381-412.
- Schott, D., E. D. Waddington, and C. F. Raymond. 1992. *Journal of Glaciology* **38**, 162-168.
- Shoji, H., and Langway, C. C. 1982. *Nature* **298** (6874), 548-550.
- Shoji, H., and Langway, C. C. 1987. *J. Phys. (Paris)*, **48**, Colloq. C1, 551-556 (Supplement au 3).
- L. G. Thompson. 1977. IAHS Publication **118**, 351-364.
- Uchida, T. 1994. Private communication.
- Uchida, T., T. Hondoh, S. Mae, V. Ya. Lipenkov, and P. Duval. 1994. *Journal of Glaciology* **40**, 79-86.
- Uchida, T., T. Hondoh, S. Mae, P. Duval, and V. Ya. Lipenkov. In *Fifth Inter. Symp. on Antarctic Glaciology*, to be published, 1994.
- Weertman, J. 1968. *Journal of Geophysical Research* **73** (8), 2691-2700.
- Young, N. W., M. Pourchet, V. M. Kotlyakov, P. A. Korolev, and M. B. Dyugerov. 1982. *Ann. Glaciology* **3**, 333-338.

FIGURE CAPTIONS

1. The AMANDA high-energy neutrino observatory. The top four strings are frozen into the ice at South Pole and are working. The lower six strings will be deployed at a greater depth to be discussed in this paper.
2. Depth as a function of age for various deep cores. Curves are meant to guide the eye. Points are a sampling of more extensive data from the references in Table 1.
3. Universal curve of dimensionless depth vs dimensionless age, with $a(t) = \text{step function}$, reduced at 15-110 kyr BP (see text).
4. Models of depth as a function of age for South Pole ice. Solid curve (the AMANDA model) is for $a = 0.073$ m/yr since 15 kyr BP and $a = 0.055$ m/yr before 15 kyr BP. Dashed curve is the flowline model of McInnes and Radok (1984). Irregular curve is dust flux at Vostok after smoothing by a cubic spline function (Petit et al., 1990). The scale for dust flux is linear, with largest peak corresponding to 7.3×10^{-7} cm/yr.
5. Inverse scattering length as a function of depth for air bubbles. The data for Byrd and Vostok were taken from microscopic measurements of bubbles in cores. The AMANDA data for South Pole were based on light scattering of laser pulses in situ. The solid curve shows the effect of hydrostatic pressure on bubble sizes, assuming all of the air is trapped in bubbles. The dashed curve shows the calculated dependence on depth due to conversion of bubbles into air hydrate crystals (Price, 1994).
6. Temperature profiles for several sites in Greenland and Antarctica, compared with pressure dissociation equilibria (converted to depths) for nitrogen-clathrates and air ($\text{N}_2 + \text{O}_2$) hydrates. In the hatched region both bubbles and hydrate crystals should co-exist. The solid triangles indicate depths at which air hydrate crystals are first observed to appear; the solid squares indicate depths at which air bubbles have completely disappeared. Arrows at solid squares for Dome C and Camp Century indicate lower limits on depths for disappearance of bubbles.

Table 1. Data on Ice Cores and Drilling Sites

Location	Lateral Flow rate (m/yr)	Height, h , of flowrate transition (m)	Depth, H , to bedrock (m)	Elevation (m)	Surf. temp. ($^{\circ}$ C)	Recent accum. rate (m ice/yr)	Accum. rate 15-110 kyr BP	Bubbles obs. to disappear at:	Hydrates observed to appear at:	Depth of max. dust conc.
Camp Century ^a	3.3	430	1388	1890	-24	0.38	n.s.	>1388 m	1100 m	1200 m
Milcent ^b	48	n.s.	2340	2450	-22	0.53	n.s.	n.s.	n.s.	n.s.
GISP (Dye 3) ^c	12.3	300	2037	2479	-19.6	0.49	0.25	1540	1092	n.s.
GRIP (Summit) ^d	0	1200	3029	3238	-32	0.23	0.12	1350	n.s.	n.s.
Byrd Station ^e	12.8	?	2164	1520	-27.9	0.13	0.1	1100	727	1450
Vostok ^f	3	400	3700	3488	-55.6	0.024	0.018	1250	500	420
Dome C ^g	0	?	3700	3240	-53.5	0.037	0.028	>800	n.s.	600
South Pole	8-10 ^h	400-800 ^h	2900	2835	-51	0.073 ⁱ	0.055	>1000; predict ~1450	predict ~500	predict ~1000

- a. Dansgaard and Johnsen (1969); Dansgaard and others (1982); Hammer and others (1978).
b. Hammer and others (1978).
c. Dahl-Jensen and Johnsen (1986); Dansgaard and others (1982).
d. Schott and others (1992); Dahl-Jensen (1989); Dansgaard and others (1993).
e. Robin (1983); Lorius and others (1984).
f. Ritz (1989); Lorius and others (1985); Jouzel and others (1993); De Angelis and others (1984).
g. Lorius and others (1979); J.-R. Petit and others (1981).
h. Koci (1994).
i. Mosley-Thompson and Thompson (1982); Giovinetto (1964); Young and others (1982).

Table 2. Dust Concentration in Cores at Depths for Holocene, LGM, and 40 kyr BP

Location	Holocene	LGM	40 kyr BP	Ref.
Camp Cent.	2400	2×10^5	not studied	a
Summit	1×10^4	not studied	not studied	b
Byrd	1000	1×10^4	1500/ml	a
Dome C	4200	7×10^4	1.1×10^4 *	c
Vostok	5650	6.5×10^4	1.6×10^4	d
South Pole	1450	predict 1.9×10^4	predict 3350	e

*Measurement made near bottom of core, at ~ 30 kyr BP.

(a) L.G. Thompson (1977); (b) Palais *et al.* (1992); (c) Petit *et al.* (1981); (d) De Angelis *et al.* (1984); (e) Gayley and Ram (1985); E. Mosley-Thompson (1994).

Table 3. Size Distribution of Dust in a South Pole Core at Depth of 100 - 349 m

Diameter (μm)	No./ml *	Area/ml
0.1 - 0.4	6×10^4	$1.7 \times 10^{-5} \text{ cm}^{-1}$
0.4 - 0.8	8200	2×10^{-5}
0.81 - 1.0	885	6×10^{-6}
1.01 - 1.25	578	6×10^{-6}
1.26 - 1.59	343	5.5×10^{-6}
1.6 - 2.0	190	5×10^{-6}
≥ 2.0	235	1.2×10^{-5}
≥ 0.1	7×10^4	7×10^{-5}

*Gayley and Ram (1985); Mosley-Thompson (1994).

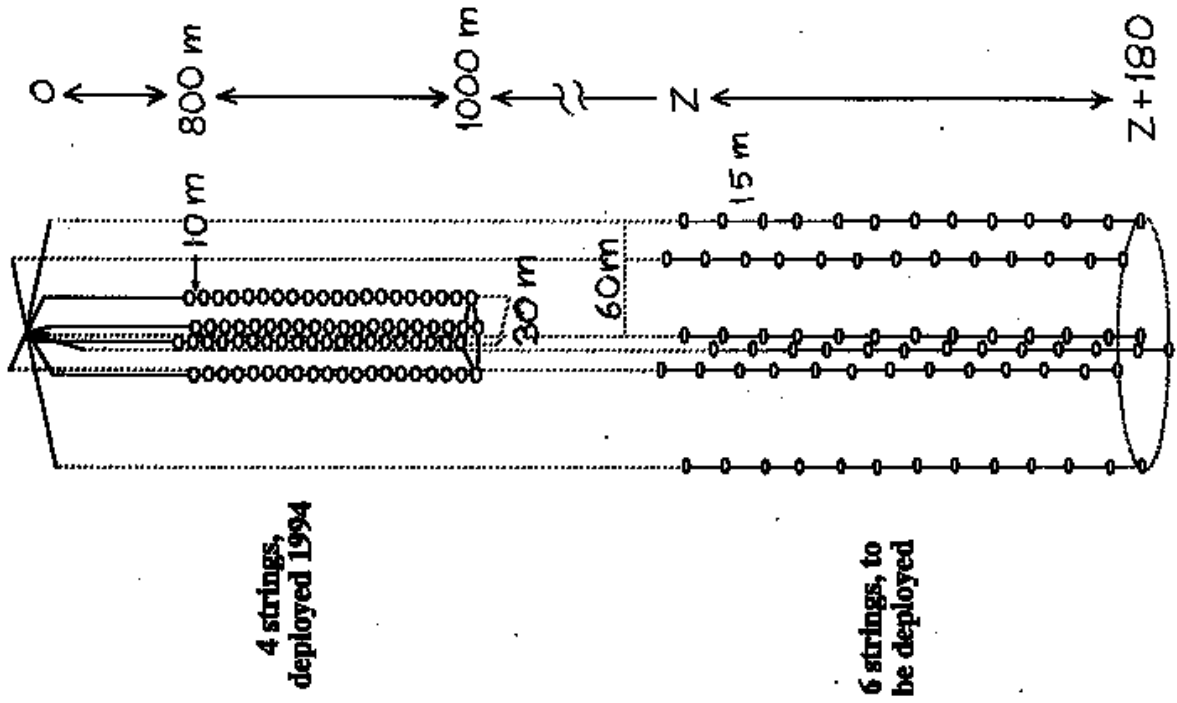


Fig. 1

This figure "fig1-1.png" is available in "png" format from:

<http://arxiv.org/ps/astro-ph/9501072v2>

This figure "fig2-1.png" is available in "png" format from:

<http://arxiv.org/ps/astro-ph/9501072v2>

This figure "fig3-1.png" is available in "png" format from:

<http://arxiv.org/ps/astro-ph/9501072v2>

This figure "fig4-1.png" is available in "png" format from:

<http://arxiv.org/ps/astro-ph/9501072v2>

This figure "fig5-1.png" is available in "png" format from:

<http://arxiv.org/ps/astro-ph/9501072v2>

This figure "fig6-1.png" is available in "png" format from:

<http://arxiv.org/ps/astro-ph/9501072v2>

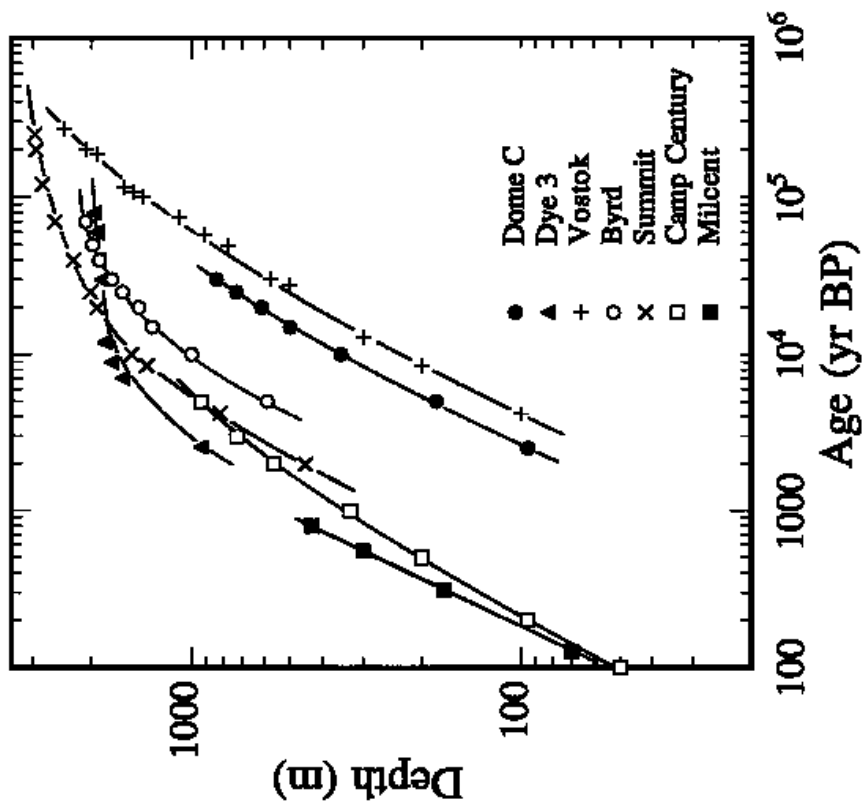


Fig.2

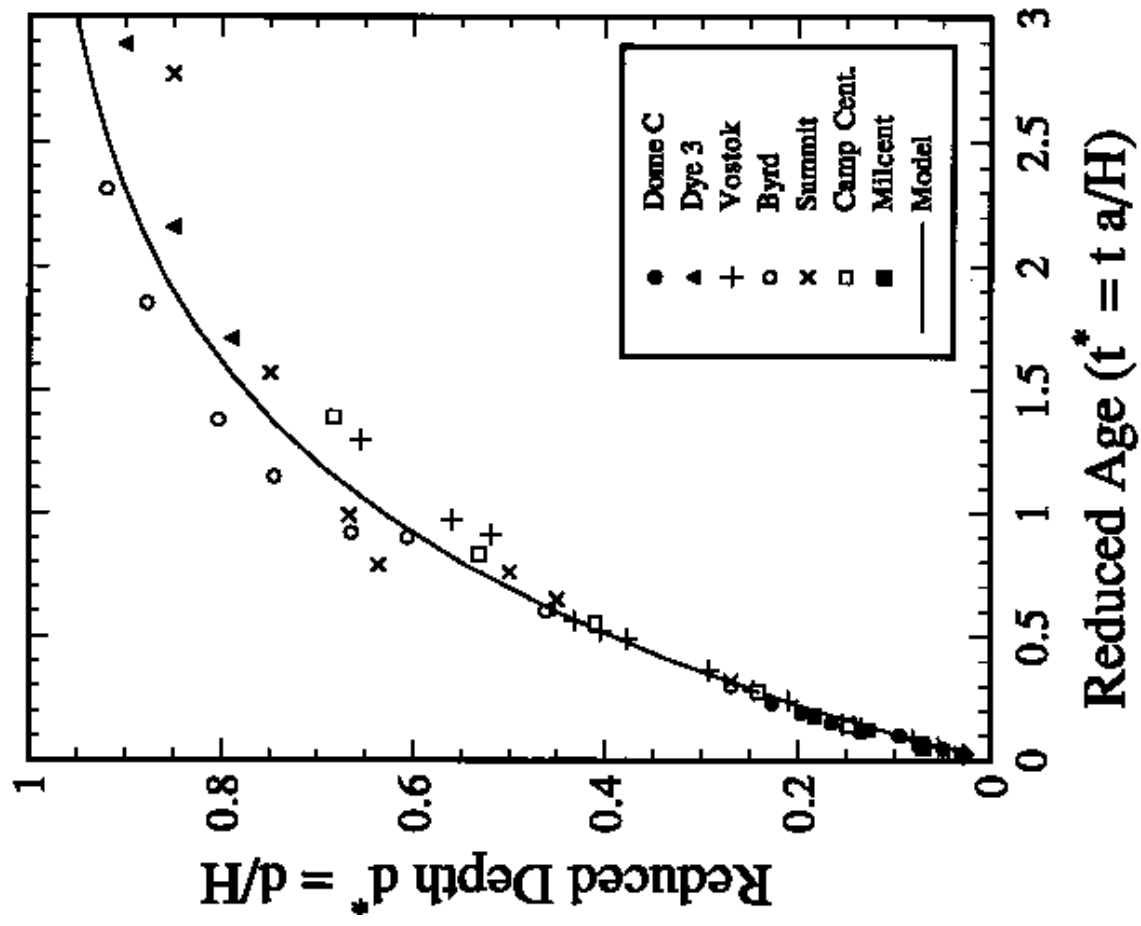
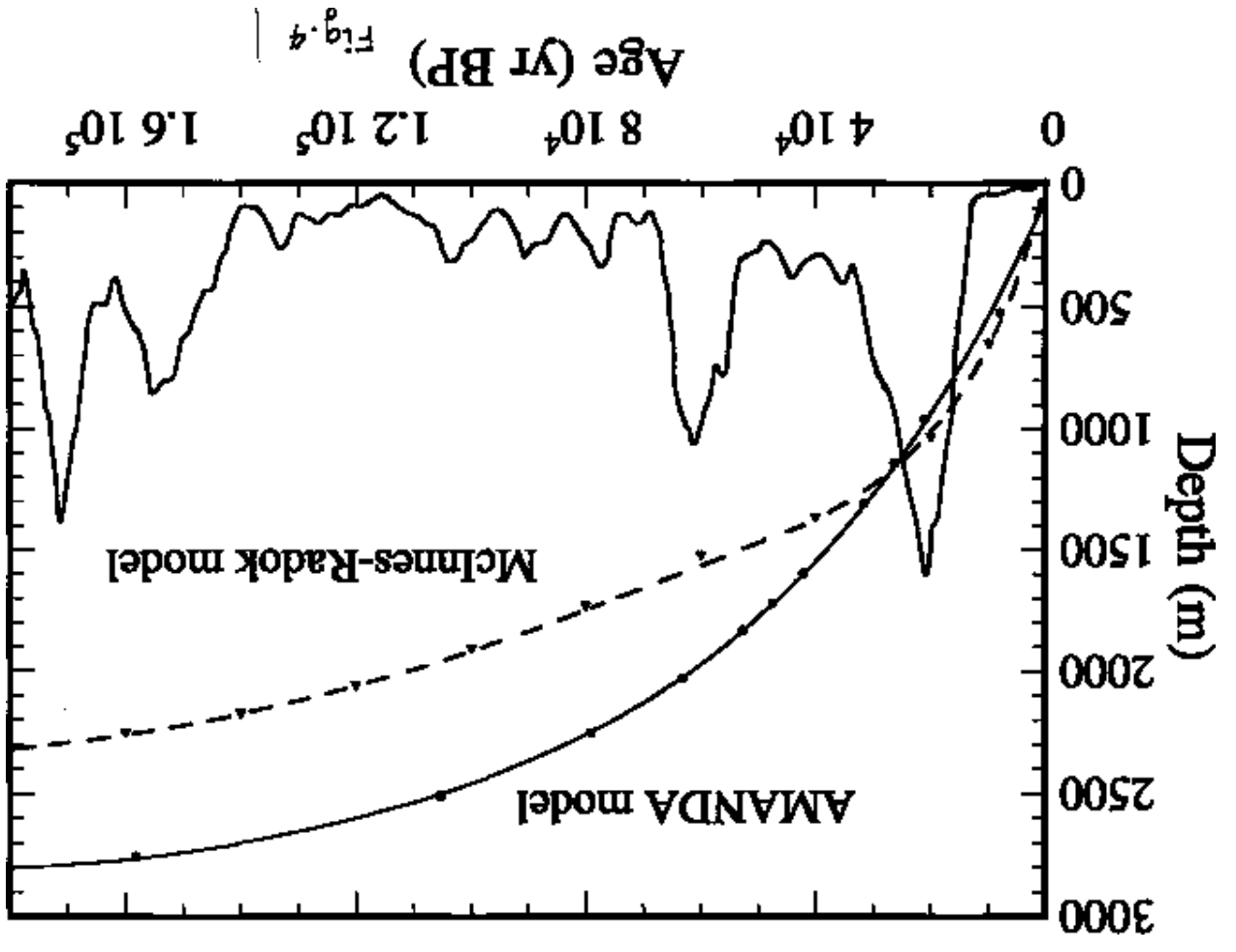


Fig.3



Age (yr BP) | Fig. 4

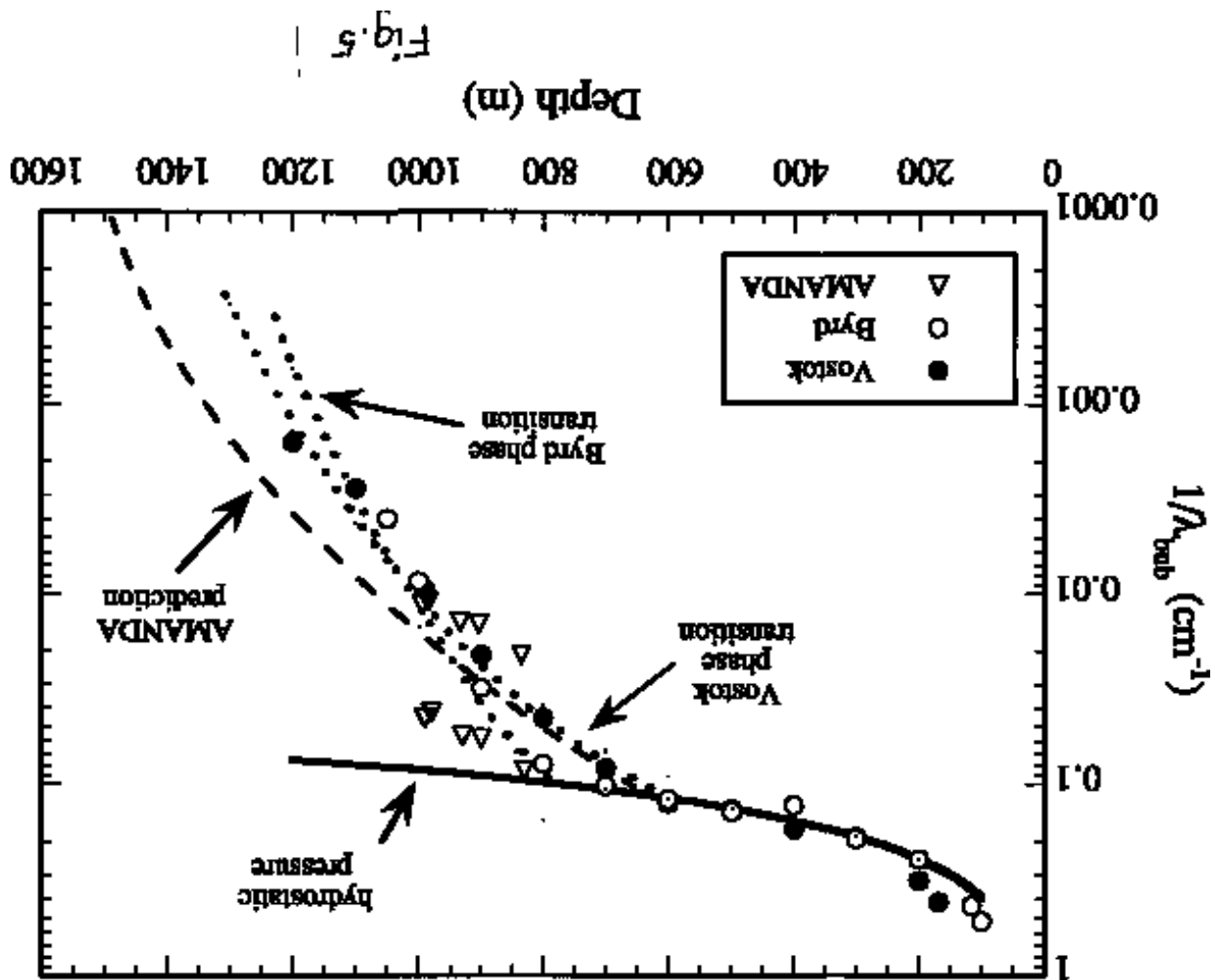


Fig. 6

